Dynamic behaviour of the weld pool in stationary GMAW

Julien Chapuis, Edward Roméro, Fabien Soulié, Cyril Bordreuil, Gilles Fras

63rd Annual Assembly & International Conference of the International Institute of Welding
11-17 July 2010, Istanbul, Turkey

Dynamic behavior of the weld pool in stationary GMAW

J. Chapuis, E. Romero, F. Soulié, C. Bordreuil and G. Fras

LMGC UMR-5508 Université Montpellier 2, 34095 Montpellier, France

julien.chapuis@lmgc.univ-montp2.fr

Abstract

Because hump formation limits welding productivity, better understanding of the humping phenomena during the welding process is needed to access process modifications that decrease the tendency for hump formation and then allow higher welding productivity. From a physical point of view, the mechanism identified is the Rayleigh instability initiated by a strong surface tension which induces a variation of kinetic flow. But the causes of the appearance of this instability have not yet been explained well enough.

Because of the phenomena complex and multi-physics, we chose as a first step to conduct an analysis of the characteristic times and lengths involved in weld pool in pulsed stationary GMAW. The goal is to study the dynamic behavior of the weld pool, using our experimental multi - physics approach. The experimental tool and methodology developed to understand these fast phenomena are presented first: frames acquisition with high speed digital camera and specific optical devices, numerical library.

The analysis of geometric parameters of the weld pool during welding operation, for several welding conditions, is presented in the last part: we observe the variations of wetting angles (or contact lines angles), the radius and the height of the weld pool ("macro-drop") versus weld time, volume of the macro drop, process energy. The results show the influence of input parameters of the system (energy, volume of wire metal) on the macro drop, and thus guide us in choosing the physical mechanisms to be considered for a future model.

Keywords: *GMAW, Weld pool, Experimental approach, Dimensional analysis, Wetting.*

1. Introduction

Industrial applications of welding processes constantly demand productivity and quality enhancements. One such approach involves using numerical simulation and experimentation in a complementary way to improve welding operations [1]. However, numerical simulations are mainly related to a specific problem such as heat transfer and distortion predictions, so an experimental method is necessary for synchronized measurement of different parameters during welding operations and correlations with numerical predictions. Thus, the main objectives of this work were: 1) to improve understanding of physical phenomena and their interactions, 2) to validate numerical simulations, and 3) to facilitate remote monitoring of arc welding using these results.

To illustrate this approach we have chosen a problem linked to productivity and quality for the manufacture of welded joints. For welded products, productivity increases with welding travel speed, but some welding defects related to bead shape, such as formation of bead humps and undercutting at the weld edges limit the maximum feasible travel speed. Because hump formation limits welding productivity, better understanding of the humping phenomena during the welding process is needed to attempt process modifications that decrease the tendency for hump formation and allow higher productivity welding.

Bradstreet [3] was the first researcher to experimentally study bead hump formation in the gas metal arc welding (GMAW) process. Humping was defined as the series of undulations of the weld bead. From a physical point of view, the mechanism identified is the Rayleigh instability initiated by a strong surface tension which induces a variation of kinetic flow [9]. These hydrodynamic disturbances cause constrictions in the back of the weld pool. It results both in a cooling and a rapid solidification of the liquid stream that produces a boundary "solid" for the liquid metal coming upstream. A hump is then formed. Cho [4] used computer simulation to provide the knowledge of heat and fluid flows leading to a deeper understanding of humping phenomenon during the high travel speed weld. Schiaffino [5] also encountered such phenomena, but for a deposit of wax. He used an interesting physical approach based on a dimensionless analysis of stationary wax deposit. There are also two studies on the behavioral analysis of the weld pool in GMAW [6, 7 & 8]. They approach the subject mainly by numerical simulation and one experiment (with high speed camera) to validate their results.

Because of the phenomena complexity, we then chose to conduct an analysis of characteristic times and lengths

involved in the behavior of weld pool in pulsed stationary GMAW. To address this issue we have chosen to proceed in three steps: 1) Using our experimental approach, extracting data process, thermal and geometric parameters of the weld pool during welding; 2) making a dimensional analysis of the weld pool and 3) balancing the physical mechanisms identified by a dimensionless analysis. The goal is to simplify a future modeling process for a detailed understanding of the phenomenon of humping.

In this paper, we mainly deal with dimensional analysis of the weld pool, during welding, at the solidification phase and post-mortem. In a first time we define the studied system and the analysis procedure.

2. Definition of the studied system

The purpose is to study the shape and the spreading of the macro-drop according depositing droplets of feed wire with the P-GMAW process.

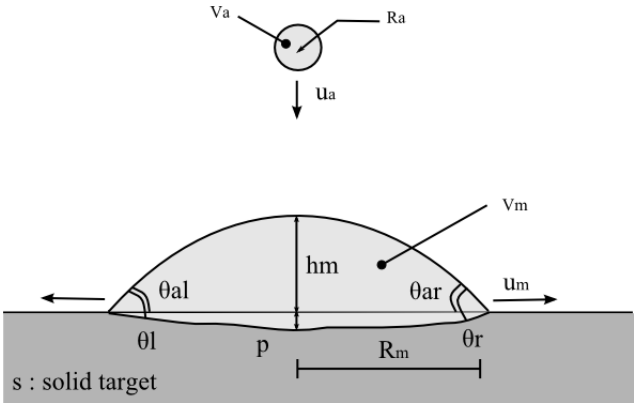

Figure 1. Macro-section of the system studied

The following indices are used to identify areas of interest: *l* = liquid, *g* = gas, *s* = solid / substrate, *a* = droplets and *m* = macro-drop. The geometry of the system studied is defined by the following quantities: *Rm* = base radius of the macro-drop, *hm* = center height of the macro-drop, *V_m* = volume of the macro-drop, *p*: maximum penetration of the macro-drop and *Θal, Θar, Θl, Θr* = wetting angles (left and right), respectively "apparent" and "real."

3. Experimental methods

We developed an accurate, reliable and synchronized measurement system in the highly noisy environment of Gas Metal Arc Welding [2]. In this case, the objective is to study the dynamic behavior of the macro-drop. We have developed an experimental procedure to automatically analyze the frames acquired with the high speed camera. To finish, we present the experimental campaign.

3.1. Experimental setup

To analyze efficiently welding and characteristic times, it is necessary to measure different kinds of signal. Welding induced a high degree of perturbation due to electromagnetic noise and radiation from the arc. Then, we have developed experimental multi-physics approach (Process, thermal, mechanic, optical …) dedicated to the study of arc processes. This approach is not limited only to a platform (figure 2) of synchronized data acquisition [11]. It also offers the possibility of easy management of the large flow of multi-physical experimental data (up to 2 Go per test) to compare and analyze them through the development of two numerical libraries open source (developed by LMGC U M R - 5 5 0 8 U M 2 - C N R S , https://subver.lmgc.univ-montp2.fr/BAME or erCv): 1) The "BAME" for all data and 2) "erCv" specific to image analysis (including the spreading of weld pool geometry during welding).

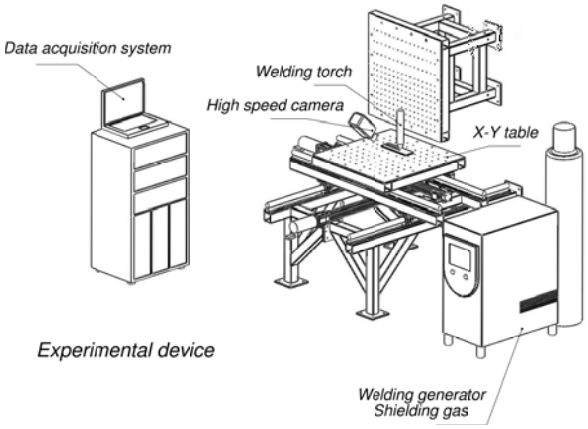

Figure 2. Experimental platform and specific devices

3.2. Analysis method

Stationary spot welds were made using the Pulsed Gas Metal Arc Welding process (Oerlikon CitoWave 500) to observe non isothermal spreading of weld pools. The target is a steel disk (thickness = 10 mm) and ER70S steel welding wire was used for welding experiments. The welding duration was 4 s. Welding parameters were set values summarized in tables 1 & 2. We have sized the target for a maximum difference of temperature of 50°C (*Rtarget* = 150mm). Our experimental approach (see section 3.1) was used to synchronize the high speed camera images, the process parameters and thermocouples acquisitions. Welding current and arc voltage were recorded at 30 kHz sampling rate. Examples of acquired current and voltage waveforms are given in figure 4, in accordance with welding parameters of the reference test. The temperature history at several locations (20 and 30 mm from the center of metal deposit), was measured with thermocouples of 0.6 mm diameter Type K wires, glued with epoxy to the plate surface. A high-speed camera (Phantom V5.0) with a back-lit shadow graphic

method recorded weld pool images at a rate of 4000 frames per second so that weld pool radius and apparent liquid-solid contact angle histories could be measured.

Table 1. Determined constant welding parameters used in experiments

Welding wire type	ER70S
Wire diameter (mm) or *dw*	1
Contact tip to work distance (mm)	20
Shielding gas flowrate (l/min)	18

A 650 ± 10nm band pass filter was used to attenuate arc light for clear images of weld pool growth and weld metal transfer. Measurements of weld pool dimensions were made using the erCv library. The erCv library was designed to facilitate the measures of the characteristic parameters (geometries and times) of evolution of a weld pool, with huge flows of processed images (up to 30,000 frames per test) [12]. An example of weld pool measurements using erCv is shown in figure 3. We can observe 8 frames from an experiment with the associated time, arc voltage and current. And in the right of the figure 3, we have the detected profiles of the weld pool.

Now, we can determine the geometric parameters (such as figure 1), for the dimensional and the dimensionless analysis. In order to do this, we have developed several functions (linked with the BAME and erCv). For example, we take the apparent wetting angle measures with linear regression or least square (parabolic, ellipse, circle) on the filtered profile drop. After that, it is easy to loop this method for all frames of the test. (More than 1000 frames per experiment), and compute the energy, volume versus the welding time. We can see the example of the spreading of the weld pool radius during welding operation (figure 5). To validate this procedure, we compare manual and automatic measures (see figure 3). These results show the ability of this data extraction method.

Table 2. Variable welding parameters used in experiments

Welding times (s)	4 to 8
Wire feed speed (m/min) or *Ws*	6 to 10
Frequency (Hz)	40 to 200
Subtract temperature (°C)	20 to 600
Shielding gas (Argon + *% CO_2*)	8 to 30

The test campaign began by a reference test. The parameters of this experiment are: welding time = 4s, wire feed speed = 6 m/min, frequency of droplets = 113 Hz, temperature of subtract = 20°C and the percentage of CO_2 = 8 (so 92 % Argon). Then to study the behavior of the macro drop, we vary several parameters as those cited for the reference test. We can see the choice of these different parameters in table 2.

4. Results

The analysis of the reference test is presented first, beginning with the comment of acquired data, and the dimensional analysis of the macro drop. In a second part, we observe the influence of parameters variation (table 2).

4.1. Reference test analysis

The reference test was realized four times to ensure repeatability; the results indicate that it is correct.

Figure 4 shows acquired data during welding (left) and the post-mortem macro drop result (right). The arc voltage and current signals show the type of welding current (pulsed). These signals also allow us to control the stability of the metal transfer (no short circuit noise) and gives access to weld energy at the source during the experiment. The signals of four thermocouples are also included. We can see that the thermocouples 2 and 3 show an imperfect axisymmetry of the macro drop. The imperfect axisymmetry remains valid only during the welding phase (probably due to a positioning error of about 1-2 mm). During the solidification phase the thermal equilibrium is quickly reached (about 80 s). The thermocouples 3 and 4 give us access to characteristic time of thermal diffusion of the studied system (about 8 s). The thermocouple signal 1 (facing backward) continues to grow over 3 s after the extinction of the arc, which gives a thermal gradient in the thickness direction of the target. The images from the high speed camera are sequenced in three phases: 1) arc ignition with great instability of process, short circuit, metal spatters (like a globular transfer), the droplet takes a lot of movement in the macro drop (volume of the droplet close to that of the macro drop, at 1 s). 2) Pulsed transfer established, the macro drop evolves until the extinction of the arc (at 4 s). During this phase, the droplet leads heat and mass but little mechanical momentum to the system. 3) Solidification phase, in which we can observe the solidification front from subtract to the top of the macro-drop. Still in figure 4, a section and a top view of a target are illustrated. This section shows a low penetration of the molten zone, but more important at the center. Hence the confirmation that we have two wetting angles: apparent (during welding operation) and real (which is slightly penetrating). We also see a collapse of the spherical cap in the center after solidification. This phenomenon is explained by axisymmetric solidification shrinkage. There were also some experiments with degassing, leading to the possible formation of columnar cavities in the center of the macro-drop.

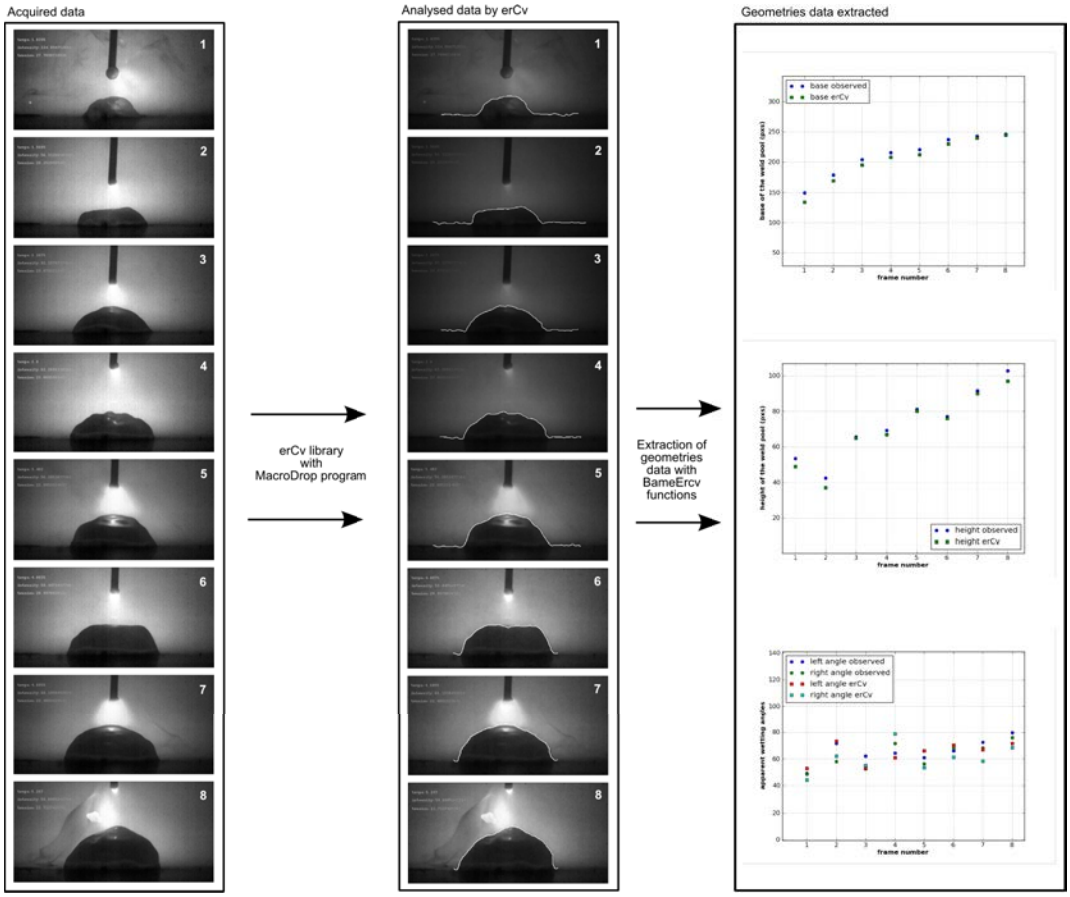

Figure 3. Weld pool measurements using erCv; the white curve represents the profile of the drop automatically detected

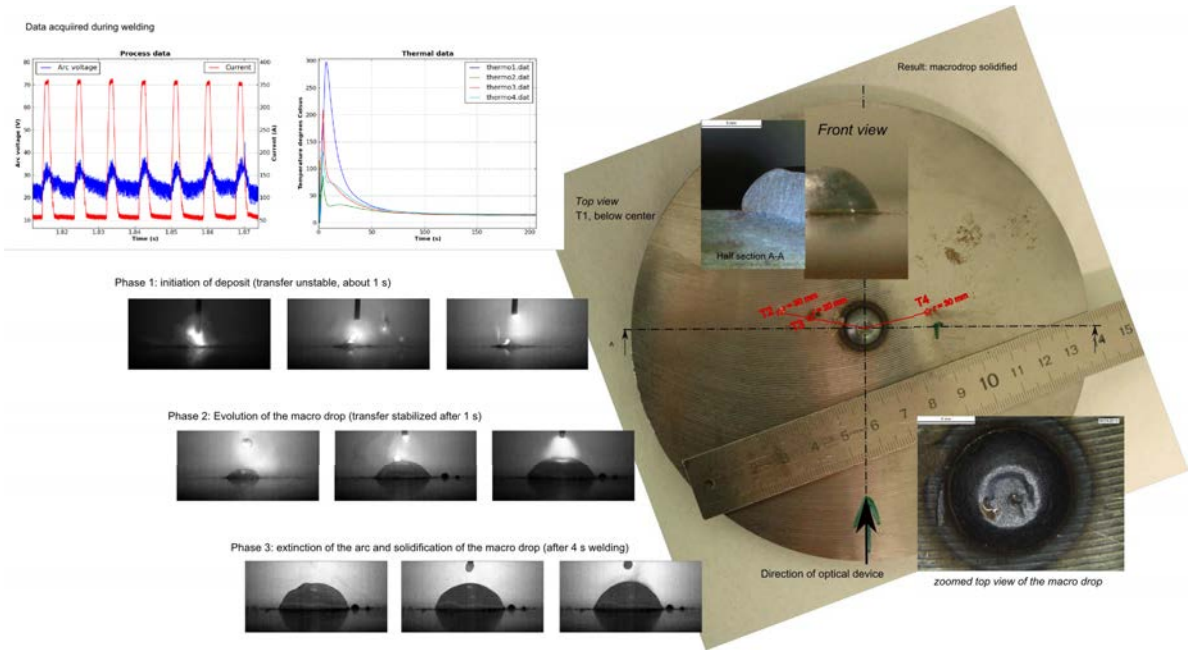

Figure 4. Experimental data of reference test

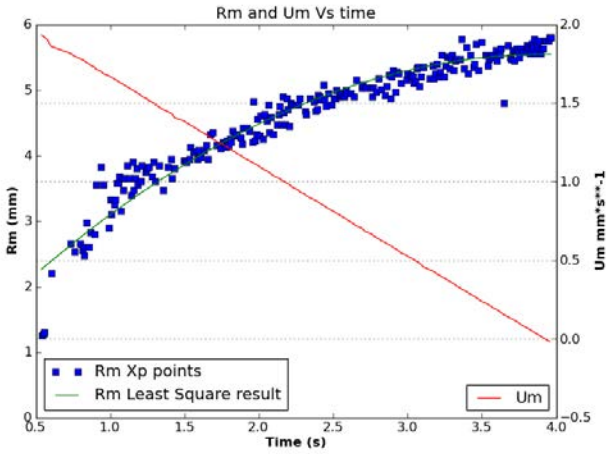

Figure 5. Diagram of radius and its rate of progression during welding

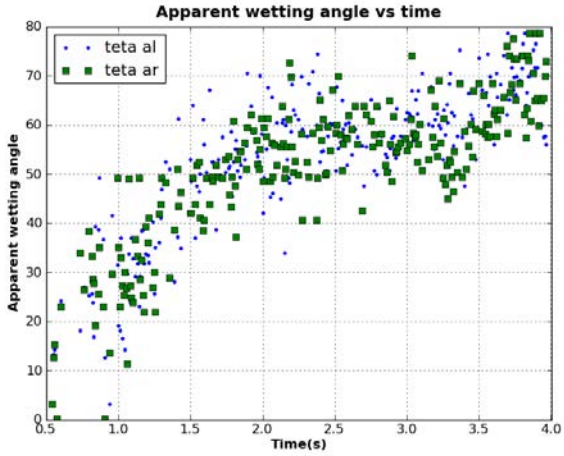

Figure 6. Diagram of apparent wetting angles vs. welding time

In figure 5, the deposit radius (*Rm*) of weld pool obtained with erCv video measurements is plotted vs. weld time. According to the experimental result, the deposit radius rapidly increased at the beginning of the weld. This is presumed to correspond to rapid spreading of the solidus isotherm on the substrate surface by direct arc heating allowing spreading of the molten metal deposit. The spreading quickly transitions to a more gradual increase. In the experimental deposit radius curve, the initial molten metal radius quickly reached 3.5 mm. After approximately 1 s of welding, we actually observe a regular spreading of the deposit radius until the extinction of the arc. The weld pool oscillations cause periodic arrest of the average radius deposit. After the extinction of arc, there is no variation of radius deposit, this phase corresponds to the beginning of solidification. The capillary effect seems thus to be preponderant over inertial effect. The radius curve is close to a quadratic function; we can deduce with a least square method the closest function and so deduce the evolution of velocity *Um* (only valid for the regular spreading phase). The result is plotted in figure 5.

Figure 6 presents the variation of left and right apparent wetting angles as a function of time. The variations are quite the same for both wetting angles according to the symmetric configuration of welding. Once again, we can observe a very quick increase of values of wetting angles in the first 1.5 s of welding. In a second phase there is a fluctuation of apparent contact angle from approximately 40° to 80°.

All these measures clearly show the existence of two phases: 1) a first one (for weld time < 1 s) corresponds to the initiation and establishment of the weld pool; 2) a second one (weld time > 1 s) corresponds to a regular growth of weld pool with metal deposit.

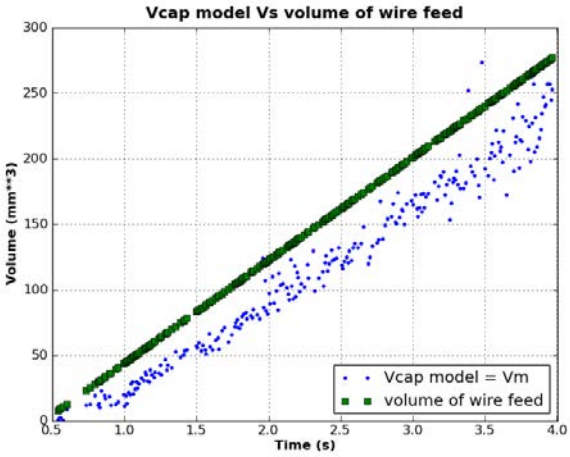

Figure 7. Comparison between the volume of feed wire and the volume of the macro-drop

In figure 7, we compare the volume of feed wire vs. the volume of the macro-drop (*Vm*). The volume of feed wire (1) is computed based on the experiment time for a wire metal speed = 6 m/min. To compute *Vm*, we consider a spherical cap model (2). We introduce *hm* and *Rm* experimentally obtained vs. welding time. Results concord. We therefore keep the spherical cap model for calculating *Vm* for further study.

$$V_{wm}(t) = \frac{\pi}{240} d_w \cdot W_s \cdot t \qquad (1)$$

$$V_m(t) \approx V_{cap}(t) = \frac{\pi}{6} h_m(t)\left(\frac{3}{2} R_m(t)^2 + h_m(t)^2\right) \qquad (2)$$

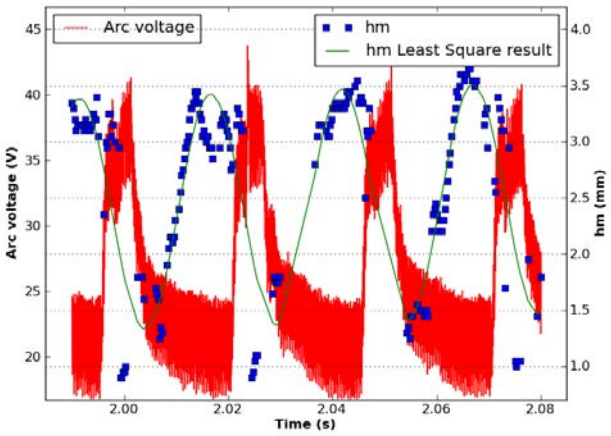

Figure 8. Comparison between hm and arc voltage

The result presented in figure 8, is a test performed with a pulse frequency of 40 Hz. The height (*hm*) oscillates at the same frequency of the arc voltage (3).

$$h_m(t) = 1.7t + \cos(2\pi \cdot F_{pulse} \cdot t + 5.6) - 1 \qquad (3)$$

We can see that the variation of the macro-drop height follows an opposite evolution to the arc voltage one. Empirically, there is a consensus that the arc length is proportional to the arc voltage (higher voltage, higher arc length). The obtained result confirms this tendency. Does the fact that the macro-drop settles after pulse mean that there is a variation of the ions flow (reversed polarity in GMAW) or that heated air volume between the electrodes causes an expansion of this volume and exerts pressure on the macro-drop?

4.2. Multi-test analysis

In this section we compare the results of all experiments listed in table 2.

For the three welding times, we find the same first phase and a second phase increasing linearly with the duration of the experiment. The duration of the welding operation has no influence on the dynamic behavior of the macro-drop.

Figure 9 shows the evolution of the radius (*Rm*) depending on the height (*hm*) of the macro-drop and for four wire feed speeds (*Ws* = 4, 6, 8 and 10 m / min). We note that the height tends to decrease while the radius increases with a faster wire feed speed. When increasing the wire feed speed, we increase both the volume of wire feed and the welding energy. This would indicate that the macro-drop with the most important energy and volume is wider, less high, and with smaller wetting angles. The effects of capillarity and inertia seem to be competing.

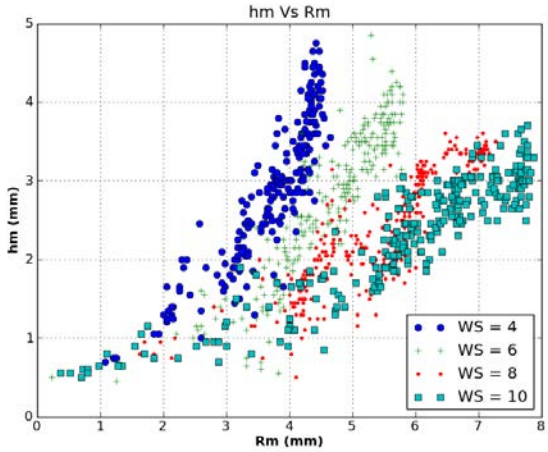

Figure 9. Diagram of the height vs. the radius of the macro-drop

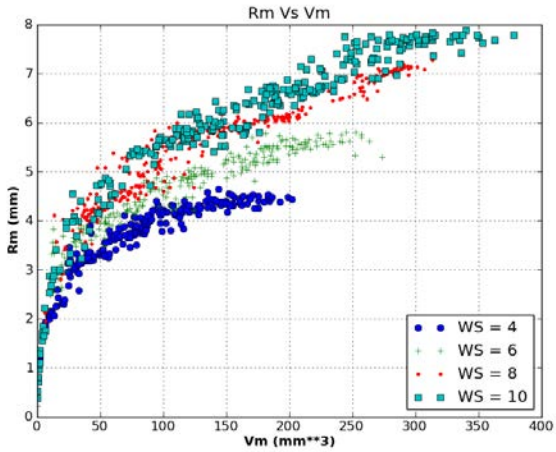

Figure 10. Diagram of radius vs. Volume of the macro-drop

It is interesting to plot *Rm* vs. the volume of the macro-drop (*Vm*) during welding (figure 10). During the first phase we find the same behavior. During the second phase the four curves diverge to a same volume of macro-drop. For a same volume (*Vm*), the radius increases with the wire feed speed.

In figure 11, we note that for a same *Vm*, the power increases with the wire feed speed. It would bring more heat to the same volume of metal, which explains the largest wetting or larger radius.

The results for experiments using different pulse frequencies (droplets and current) show no influence on the overall behavior of the macro-drop. The final geometry remains unchanged.

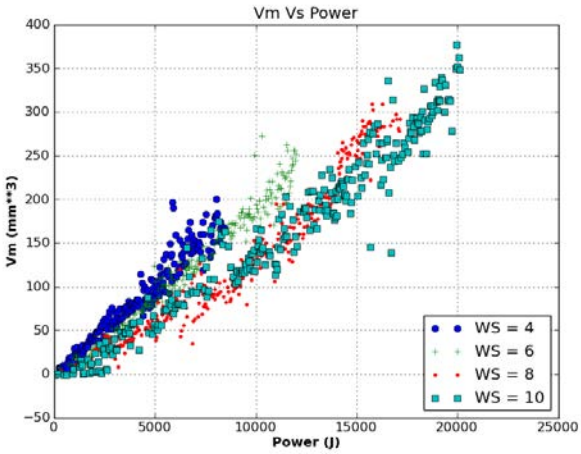

Figure 11. Diagram of Vm vs. power

In figure 12, we observe the evolution of the apparent wetting angle for three temperatures of subtract. The diagram shows that the wetting improves with the preheating temperature of the target. Beyond 300 °C, the preheating temperature of the target has less influence on the wetting angles. We observe that when preheating the disc or with a higher wire feed speed (as the welding energy), the weld pool widens and decreases in height. It seems that viscosity and surface tension effects could be in competition.

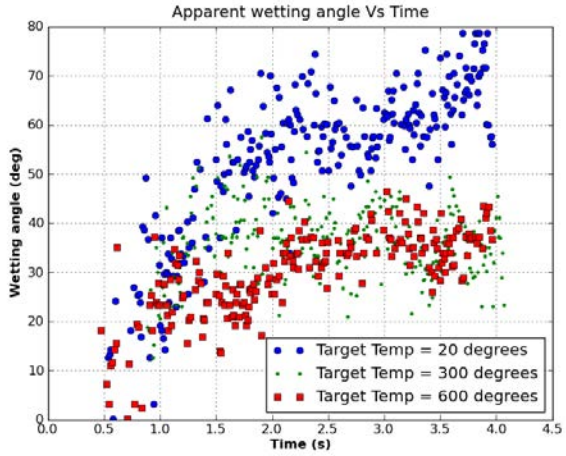

Figure 12. Diagram apparent wetting angle vs. Time for several subtract temperatures

The last experiments consisted in changing the shielding gas. For this we gradually increased the percentage of CO_2. The CO_2 has the effect of improving the wetting, but generates instabilities in the transfer of droplets. The propagation speed of the liquid front is identical for all these tests (*% CO_2*). The weld pool with 100% argon can reach apparent wetting angles higher than 90°.

4.3. Discussion

The dimensional quantities specific to the droplet transfer are not exposed in this paper. Just for information, first results give an average *Ua* = 1000 mm / min and a mean radius of the droplet (*Ra*) of 0.6 mm, these two quantities are related to the reference experiment. At this time, we have robust access to dimensional quantities of the macro-drop (*Rm*, *Um*, *hm*, *Vm* …). The analysis presented in section 4 corresponds to the study of the overall behavior of the macro-drop. A scale analysis of a period will be necessary to reveal the levels of weld pool spreading.

The spherical cap geometry model suits the macro-drop. The evolution of the parameters *hm* and *Rm* are obtained through the automatic method (see section 3.2) of two dimension images acquired during welding. These same parameters are introduced into the equation 3. The figure 7 confirms the volumic axisymmetry in addition to that observed for a thermal point of view (presented in section 4.1). The constant gap between *Vw* and *Vm* is the result of an unstable first phase (like a globular transfer, spatters). The overall results (presented in section 4.1 and 4.2) suggest a competition between the gravity and capillary effects. We also note the existence of two phases: 1) a first one (for weld time < 1 s) corresponds to the initiation and establishment of the weld pool; 2) a second one (weld time > 1 s) corresponds to regular growth of weld pool with metal deposit. So we have a first characteristic time before attempting the established regime: *t1* = 1s. Another characteristic time is that of thermal diffusion in the target from the arc extinction to the temperature homogenization: *t2* = 80s. These two characteristic times illustrate very clearly the different time scales of phenomenon with which we may be confronted for welding studies.

6. Conclusion

A new experimental device was developed allowing synchronized measurements of different physical parameters during GMA welding (such as optical measurements and process parameters). This study also illustrates the ability of numerical libraries (BAME and erCv) for analyze of acquired data. The first experimental results showed the possibility to access characteristic parameters. For example, we observed that the evolution of weld pool during pulsed metal deposition was characterized by the existence of two distinct phases (a dynamic one for early weld times and a more regular one).

The results of dimensional quantities of the macro-drop showed the potential of the system for weld analysis and its complementary relation with simulations. These first results guide us in defining the physical mechanisms playing a role in the dynamic behavior of a GMAW weld pool. We count

among them for the moment: gravity, viscosity and surface tension effects. Dimensional analysis needs to be more thorough in order to extract other characteristic quantities of the studied system. Then we use these results for the dimensionless analysis.

Therefore, the experimental study during the arc welding process will be continued for a better understanding of its physical phenomena.

References

[1] Debroy T. and Davis S.A., "Physical processes in fusion welding", Reviews of Modern Physics, vol. 67, pp. 85-112, 1995.
[2] VISHAY, "Noise Control in Strain Gage Measurements", Technical report, 2007.
[3] Bradstreet B.J., "Effect of Surface Tension and Metal Flow on Weld Bead Formation", Welding Journal, pp. 314-322, July 1968.
[4] Cho M.H. and Farson D.F., "Understanding Bead Hump Formation in Gas Metal Arc Welding Using a Numerical Simulation", Metallurgical and Materials Transactions, vol. 38, pp. 305-319, 2007.
[5] Schiaffino S., "The fundamentals of molten microdrop deposition and solidification", Massachusetts Institute of Technology, Phd-Thesis, 1996.
[6] Fan H.G. and Kovacevic R., "Droplet formation, detachment, and inpingement on the molten pool in gas metal arc welding", Metallurgical and Materials Transactions, vol. 30, pp. 791-801, 1999.
[7] Lim Y.C., Farson D.F., Cho M.H. and Cho J.H., "Stationary GMAW-P weld metal deposit spreading", Science and Technology of Welding and Joining, vol. 14, pp. 626-635, 2009.
[8] Cho M.H., Lim Y.C. and Farson D.F., "Simulation of weld pool dynamics in the stationary pulsed gas metal arc welding process and final weld shape", Welding journal, pp. 271-283, December 2006.
[9] Fabbro R., Slimani S., Coste F. and Briand F., "Analysis of the various melt pool hydrodynamic regimes observed during CW ND-YAG deep penetration laser welding", in ICALEO 07 international congress, Paper 802, 2007.
[10] Planckaert J.P, " Modélisation du soudage MIG/MAG en mode short-arc.", Université Henri Poincaré, Nancy1, France, Phd-Thesis, 2008.
[11] Chapuis J., Romero E., Bordreuil C., Soulié F. and Fras G., "BAME library: A library for analyzing multi-physics data acquisitions in Welding", to be published.
[12] Romero E. and Bordreuil C., Chapuis J., Soulié F. and Fras G. " Edge detection of weld pool, macro-drop and metal transfer drop in TIG and MIG processes by a new weld image processing library: erCv", in 6 3 r d International Conference of the International Institute of Welding, Istanbul, July 2010.